INDENTATION FRACTURE: APPLICATIONS IN THE ASSESSMENT OF STRENGTH OF CERAMICS

B.R. LAWN, D.B. MARSHALL,* P. CHANTIKUL and G.R. ANSTIS

Department of Applied Physics, School of Physics,
The University of New South Wales, Kensington, N.S.W. 2033.
*Now at Materials and Molecular Research Division,
Lawrence Berkeley Laboratory, Berkeley, Calif. 94720, U.S.A.

(Received January 14, 1980)

The application of sharp-indenter fracture mechanics to strength testing of ceramics is surveyed. A routine two-step procedure forms the basis of the test: the specimen is first loaded with a Vickers indenter to introduce a well-defined "radial" crack pattern into the surface, and is then taken to fracture under flexure. Formal relations for the strength under equilibrium or fatigue conditions are obtained as a function of the indentation variables, notably the peak contact load, from a detailed theoretical analysis of the crack growth. Experimental results for soda-lime glass and several other ceramics confirm the essential predictions of the theory. The approach offers a simple and economical route to the evaluation of materials for high-strength applications, particularly in situations where severe contact events (e.g. sharp-particle impact) are likely to be experienced. Critical fracture parameters, such as toughness K_C and crack velocity exponent n, may be obtained from the strength data without any need to measure crack dimensions. Finally, the growth characteristics of the radial crack system provide physical insight into the nature of true surface flaws, particularly the role played by irreversible processes in the micromechanics of flaw evolution.

1 Introduction

The strength of ceramics (at least at room temperatures) is determined by the resistance to growth of brittle microcracks. All analyses of strength are based, in some form or other, on the two major precepts which underlie the classical Griffith theory of brittle fracture:[1] (i) brittle materials contain "flaws" which act as initiating centres for crack growth; (ii) the propagation of "well-developed" cracks proceeds in accordance with a balance between "driving" forces (associated with mechanical energy release) and "resisting" forces (associated with creation of crack surface area). Present-day fracture mechanics, which seeks to formulate the response of well-defined crack systems in terms of characteristic material parameters, is the natural end product of concerted attempts to generalise the Griffith concept so as to accommodate an infinite variety of potential test configurations. Conventionally, fracture mechanics measurements are made on large-scale, accurately machined test pieces that allow crack progress to be followed as a function of applied loading, time, environment, etc., from which empirical laws of crack growth may be evaluated.[2] Taken in conjunction with the assumption that microscopic flaws behave in a similar fashion to macroscopic cracks, along with some knowledge of how the flaws are distributed in a given ceramic component, such fracture mechanics evaluations serve as a useful basis for predicting strength characteristics under prospective service conditions.

However, the fracture mechanics approach is not without its difficulties. First, the fabrication and testing of a suitable fracture specimen requires a certain expertise — complications of specimen geometry, material microstructure, etc., can have large effects on data reproducibility.[2] Second (and perhaps more importantly), it is not always clear that large-scale-crack data do indeed suitably reflect the manner in which flaws respond under stress. Difficulties such as these provide serious obstacles in the design of components for load-bearing applications, especially in hostile environments where a long lifetime is an essential requirement.[3] The ensuing errors in prediction are of the systematic type, not readily apparent in the statistically-based procedures commonly employed to accommodate uncertainties due to flaw-size variations.

In this paper we review the capabilities of a relatively recent addition to the strength-testing repertoire for ceramic materials, indentation fracture.[4–9] The basic approach is simple: (i) a standard hardness-testing indenter is used to introduce a localised, well-defined crack pattern into the surface of a flexural test piece; (ii) with the indentation crack now acting as the controlling flaw, the test piece is taken to failure. Since the indentation crack patterns are themselves amenable to straightforward fracture mechanics analysis, the question of strength prediction is placed on a much sounder footing. Moreover, the high reproducibility in the geometry and scale of the patterns under given contact conditions eliminates the need to resort to statistical methods, with attendant economy in specimen requirements. Further, the indentation load can be varied over a sufficiently large range that the scale of fracture effectively spans the gap between macroscopic crack and microscopic flaw. Of course, adoption of any such controlled-flaw approach does not mean that the pre-existing flaw distribution is eliminated as a factor in the strength characterisation of a given material. However, as we shall demonstrate, this is only a minor consideration in the evaluation of materials for applications where the component surfaces are exposed to occasional damage-producing events, e.g. as in particle impact.

We begin by outlining the theoretical background to indentation fracture mechanics insofar as it relates to strength. Experimental results for soda-lime glass (model material) and a broad range of other ceramics are then surveyed. Finally, we discuss the implications of the approach concerning optimisation of material fracture parameters in the design of ceramics.

2 Theoretical Background

A complete analysis of the indentation fracture problem involves a detailed computation of crack evolution within a strongly inhomogeneous contact stress field.[4] Broadly, indenters may be classified as either "blunt" or "sharp", according to whether the material response about the immediate contact zone is reversible or irreversible. "Real" indentation events encountered during service operation may be considered to lie somewhere between these two extreme cases. Here we shall concentrate on sharp indenters: not only do they represent the "worst case" of surface damage, thereby satisfying the requirements of conservative design, but they also provide a great deal more information on the general mechanical behaviour of the test material. In particular, we shall take the Vickers diamond pyramid indenter as our standard configuration. Fig. 1 illustrates the essential variables in the indentation/strength sequence: our aim is to indicate briefly how one sets out to evaluate the strength in terms of these variables, appropriate to the conditions of fracture (e.g. equilibrium, kinetic, dynamic). For this purpose, it is convenient to express the driving forces for the fracture in stress-intensity-factor notation, in order that the various contributions to the field on the crack at any stage in the sequence be reduced to simple, additive quantities.[1] A key to the symbols used thoughout this paper will be found as Appendix 1.

2.1 Mechanics of the Radial Fracture System

Consider the first stage in the sequence, Fig. 1(a). A Vickers indenter produces a well-defined deformation/fracture pattern, whose scale is determined by the peak load P. The surface pattern consists of a square "plastic" impression, half-diagonal a, with "radial" crack traces emergent from each corner, characteristic

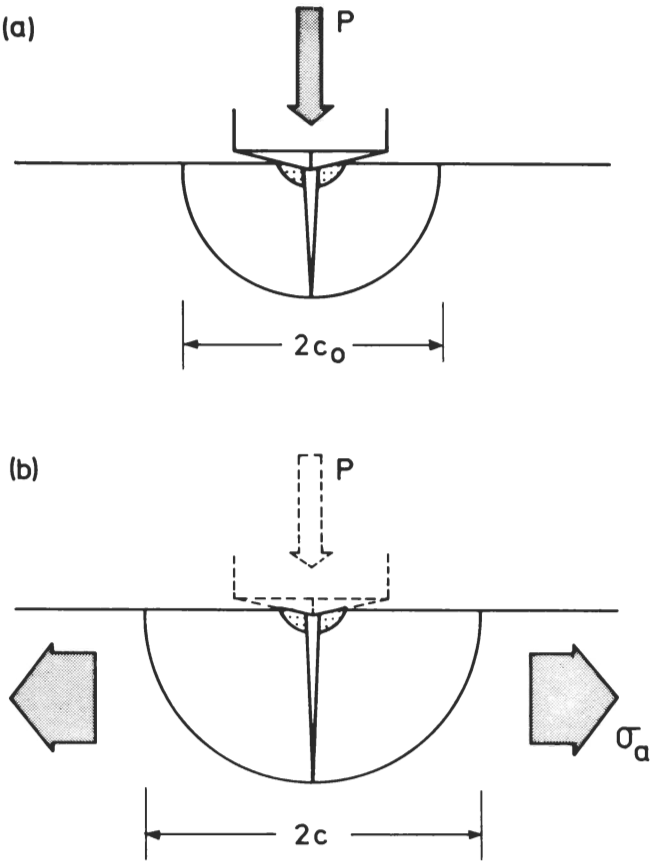

FIG. 1 Schematic of indentation/strength sequence. (a) Vickers indenter, peak load P, generates radial crack, characteristic dimension c (value c_0 immediately after contact, with post-indentation extension to c_0' if exposed to reactive environment). (b) Tensile field σ_a combines with residual contact field ("ghost contact") to drive the crack to failure configuration.

dimension c. Defining material "hardness" as the mean contact pressure, we have immediately:

$$H = P/\alpha_0 a^2 \qquad \ldots\ldots\ldots \quad (1)$$

where $\alpha_0 = 2$ for Vickers geometry; H is generally found to be load-invariant over a wide range of test conditions, and accordingly affords a useful measure of intrinsic resistance to irreversible deformation. The cracks extend beneath the surface from the radial traces as mutally intersecting, orthogonal half-pennies, as indicated in the figure; in direct analogy to Eq. (1) we obtain an expression for material "toughness":

$$K_C = P/\beta_0 c_0^{3/2} \qquad \ldots\ldots\ldots \quad (2)$$

where β_0 is a constant, thus providing a measure of resistance to fracture under equilibrium conditions. Eqs. (1) and (2) follow from dimensional analysis, and, in combination, quantify the "brittleness" of any given ceramic material.[6] The formulation to this point requires no explicit knowledge of the actual mechanisms of deformation or fracture evolution.

A second system of cracks, the so-called "lateral" cracks (not shown in Fig. 1), generally accompanies the radial system. These cracks spread sideways from the deformation zone, beneath the indentation surface, and tend to cause chipping[10]. While their cumulative effect in multi-particle contact is a major consideration in the erosion properties of ceramics, the laterals do not penetrate downward into the bulk of the material, and hence do not contribute in any direct way to the strength. They accordingly receive no further attention in this paper.

The actual manner in which the radial crack system evolves during the contact cycle is complex, but must be considered if the mechanical response in subsequent tensile loading is to be understood. By virtue of the plastic contact process, the field which drives the cracks contains both an elastic (reversible) and a residual (irreversible) component.[7,8] Of these, it is the residual component which is the more important, for growth into the half-penny configuration proceeds to completion as the indenter is *unloaded*. The elastic field at the indentation surface is in fact compressive, and accordingly acts as a restraint on radial expansion until the load is removed. Thus the final crack is subject to a continuing driving force, which may be characterised by a residual stress intensity factor for penny-like geometries[7]:

$$K_r = \chi_r P/c^{3/2} \qquad \ldots\ldots\ldots \quad (3)$$

where χ_r is a constant. Detailed analysis of the contact process shows that the "constant" depends on other factors[9]:

$$\chi_r = \S^R (E/H)^{1/2} (\cot\psi)^{2/3} \qquad \ldots\ldots\ldots \quad (4)$$

where E/H is the ratio of Young's modulus to hardness, ψ is a characteristic half-angle for the indenter (74° for Vickers), and $\S^R$ is another constant for radial cracks. Special note may be made of the E/H term, which enters via the requirement that plastic distortions at the contact zone be accommodated by the surrounding elastic matrix; "softer" materials, i.e. those with low values of H/E, will clearly experience greater residual driving forces. Hence in dealing with the fracture properties of ostensibly brittle ceramics it becomes necessary to give some consideration to the deformation responses as well. This conclusion extends to the crack *origins;* the threshold for radial initiation is largely independent of pre-existent flaw population, indicating that the contact deformation generates its own incipient flaws[11].

Equations (3) and (4) constitute the basis for any post-indentation fracture analysis. Under conditions of equilibrium fracture, the unloaded radial cracks remain stable at $K_r = K_C$; with c_0 the characteristic dimension appropriate to this configuration, the empirical constant β_0 in Eq. (2) identifies with the quantity χ_r^{-1}. Such conditions may be approximated even under impact conditions, provided the contact rate is small compared to the velocity of stress waves ("quasistatic approximation"); the peak impulsive load is then determined by the kinetic energy U_K of the incident indenter[12]:

$$P = (9\,\alpha_0\, H \tan^2\psi)^{1/3}\, U_K^{2/3} \qquad \ldots\ldots\ldots \quad (5)$$

If the contact surface is exposed to a reactive chemical environment, the system is subject to further, subcritical expansion at $K_r < K_C$, in which case a non-equilibrium crack dimension $c_0' > c_0$ obtains. As we shall see, what happens to the crack between indentation and subsequent tensile loading is of little consequence insofar as strength is concerned; it is the severity of the contact event, as quantified by the load P, which emerges as the controlling factor.

Implicit in the above analysis are several assumptions concerning the state of the test material. Variations in the microstructure, and the absence of extraneous stresses prior to contact, are important examples. These factors are expected to be reflected in the radial crack configuration, and will be examined briefly in our experimental investigations of the strength characteristics.

2.2 Mechanics of Failure from Radial Flaw

Consider now the second stage in the indentation/strength sequence, Fig. 1b. The radial crack system is subjected to a tensile stress σ_a, which is increased until a failure instability is attained. The stress intensity factor appropriate to this tensile loading is of the standard form[1]:

$$K_a = \sigma_a(\pi\Omega c)^{1/2} \qquad \ldots\ldots\ldots \quad (6)$$

where Ω is a crack-geometry constant. This term augments the residual driving force on the system from the preceding indentation event, Eq. (3), so the *net* stress intensity factor is:

$$K = \chi_r P/c^{3/2} + \sigma_a(\pi\Omega c)^{1/2} \qquad (c > c_0') \quad \ldots\ldots\ldots \quad (7)$$

It is noted that the residual term dominates at small c (reflecting the localised nature of the responsible contact deformation processes), and must therefore be expected to exert a significant influence on the strength.

We now investigate the mechanics of failure under both equilibrium ("inert" strength) and non-equilibrium ("fatigue" strength) conditions.

TABLE 1

Ceramic Materials Used in This Study*

Material	Source	Geometry	E/GPa	H/GPa	K_C/MPa m$^{1/2}$
Soda-lime glass	Commercial sheet	Disc	70	5.5	0.75
Al_2O_3 (AD 999)	Coors Porcelain Co.	Disc	386	20.1	3.1
Al_2O_3 (AD 90)	Coors Porcelain Co.	Disc	269	13.1	3.0
Al_2O_3 (AlSiMag 614)	3M Co. (untreated)	Rod	300	14.8	3.5
	Ceramic Finishing Co. (oil-quenched)				
Al_2O_3	Freiderichsfeld Co.	Bar	360	15.1	3.2
Si_3N_4 (NC 132)	Norton Co.	Bar	370	18.5	5.5
Si_3N_4 (NC 350)	Norton Co.	Bar	170	9.6	2.0
SiC (NC 203)	Norton Co.	Bar	457	24	4.0
ZrO_2 (CaO-stabilised)	C.S.I.R.O. (Materials Science)	Bar	207	10.0	6.5
Pyroceram (C9606)	Corning Glass	Bar	120	8.4	2.5

* Material parameters are literature values. Uncertainty in K_C taken as ≈ 20%.

(a) *Equilibrium strength*

If a radial crack extends in accordance with the equilibrium requirement $K = K_C$ at all points prior to failure, Eq. (7) yields an explicit solution for the applied stress as a function of crack size,

$$\sigma_a = [K_C/(\pi\Omega c)^{1/2}]\,[1 - \chi_r P/K_C c^{3/2}] \quad \ldots\ldots\ldots \quad (8)$$

This function passes through a maximum ($d\sigma_a/dc = 0$) at:

$$\sigma_m = 3K_C/4(\pi\Omega c_m)^{1/2} \quad \ldots\ldots\ldots \quad (9a)$$

$$c_m = (4\chi_r P/K_C)^{2/3} \quad \ldots\ldots\ldots \quad (9b)$$

Comparing Eq. (9b) with Eq. (2), and recalling the inverse relation between β_0 and χ_r, it follows that $c_m/c_0 = 4^{2/3} = 2.52$. Thus the indentation crack undergoes substantial precursor stable growth, from c_0 to c_m, in achieving an instability configuration at $\sigma_a = \sigma_m = \sigma$, where σ now defines the strength. The existence of this "energy barrier" to failure has been confirmed by direct observation of radial crack growth in glass under inert conditions (vacuum, dry N_2 environment).[8] A feature of this behaviour is the uniqueness of σ_m; thus the strength is independent of whether the initial crack size corresponds to the true equilibrium value c_0 or to a larger value c_0' due to chemical enhancement prior to tensile loading (provided that $c_0' < c_m$). This conclusion runs counter to conventional strength theory based on "ideal" Griffith flaws (i.e. no residual stresses), in which flaw history can be a controlling factor.

Equations (9a) and (9b) may now be combined with Eq. (4) to obtain the equilibrium strength as a unique function of indentation load for any specified indenter/specimen system:

$$\sigma = \left\{[27(\tan\psi)^{2/3}/256\ \S^R(\pi\Omega)^{3/2}]\,[K_C^4(H/E)^{1/2}]\right\}^{1/3} P^{1/3} \quad . \quad (10)$$

This relation contains geometrical parameters for characterising the indenter (ψ) and the crack (Ω), and material parameters (K_C, H/E) for characterising the specimen response. With regard to the latter, toughness is clearly the dominant quantity. It is to be noted that Eq. (10) is independent of flaw size, consistent with our remarks in the preceding paragraph — it is the load which uniquely determines flaw severity.

The analysis outlined above is readily generalised to seemingly more complex situations. For instance, if the indentation surface were to be pre-stressed in biaxial compression, as in tempered glasses, it would be necessary only to replace σ in Eq. (10) with $\sigma - \sigma_R$, where σ_R is the magnitude of the tempering stress[8]. Or, if contact were to occur by sharp-particle impact, Eq. (5) could be used to eliminate P in favour of energy U_K[12].

(b) *Fatigue strength*

Suppose now the radial crack system is exposed to a reactive environment during the actual strength test, so that fracture occurs under kinetic conditions, i.e. in accordance with some crack-velocity function $v(K)$. Then strength tends to diminish with the duration under load, depending on the time variation of the applied stress, $\sigma_a = \sigma_a(t)$. Adopting the empirical crack-velocity function used most widely in the analysis of such "fatigue" behaviour[3], namely $v = v_0(K/K_C)^n$, Eq. (7) may be incorporated into a differential equation for crack size in terms of time[13]:

$$\dot{c}/v_0 = \left\{[\chi_r/K_C]\,P/c^{3/2} + [(\pi\Omega)^{1/2}/K_C]\,c^{1/2}\,\sigma_a(t)\right\}^n \quad \ldots\ldots \quad (11)$$

This equation has to be integrated (generally, numerically) between $c = c_0$ (or c_0', whichever is appropriate) at $t = 0$ and $c = c_f$ (final, unstable configuration, root of Eq. (7) at $K = K_C$ for which $dK/dc > 0$) at $t = t_f$ (time to failure)[13]. The two most important practical cases correspond to the stress/time functions σ_a = const. ("static fatigue") and $\sigma_a = \dot{\sigma}_a t$ at $\dot{\sigma}_a$ = const. ("dynamic fatigue").

3 Experimental Results

The indentation/strength sequence depicted in Fig. 1 is readily amenable to routine testing methods. Demands on specimen preparation are minimal — the major requirement is that the specimen geometry be suitable for flexural testing (e.g. bars, rods, discs). Each test piece is indented at the centre of its prospective tensile surface with a Vickers diamond, at a prescribed peak load. The indented test pieces are then taken to failure in flexure, standard elasticity formulae[14] being used to evaluate the appropriate strengths. Most of the tests to be described here were conducted under essentially equilibrium fracture conditions; these conditions were achieved simply by covering the intended contact site with a drop of immersion oil (inert environment) prior to testing. For certain tests, e.g. those involving particle impact and fatigue conditions, minor modifications to the above procedure had to be made. As indicated in the previous theoretical sections, no detailed examination of the radial cracks responsible for the failures was necessary. Cursory inspections of the fracture surfaces were nevertheless made in several cases, especially in those specimens indented at relatively low loads, to ascertain whether failure originated at the indentation crack or at some pre-existent flaw.

In the following, we describe the experimental indentation/strength characteristics for a range of ceramics (Table 1), taking soda-lime glass as a model material for special consideration. Our immediate concern will be to confirm the essential predictions of the theory for each of the material systems considered; implications of the results in relation to evaluation of basic material parameters will be dealt with in the Discussion.

3.1 Soda-Lime Glass

Indentation/strength data are shown for soda-lime glass discs in Figs. 2-4, representing a variety of test conditions. Fig. 2 shows the equilibrium strength as a function of contact load for thermally tempered (surface compressive stress σ_R = 128 MPa) and annealed (σ_R = 0) discs[15]. In the region of "high" loads, where the indentation crack system dominates the pre-existent flaw population, a linear fit of slope −1/3 may be made to the logarithmic data plot for the annealed glass, in accordance with Eq. (10). In the same load region, the corresponding curve for the tempered glass is generated by translating the fitted function at σ_R = 0 vertically upward by an amount 128 MPa for all values of P. At "low" loads a strength "cutoff" occurs, indicating dominance of the pre-existent flaws. It is noted that the prior defect state of the specimen surface, i.e. as-received vs grit-blasted (SiC particles), is an important factor in the low-load region only, consistent with the theoretical predictions of Sect. 2.2.

Fig. 3 is a similar plot, but for specimens subjected to particle impact rather than static indentation as the essential contact step

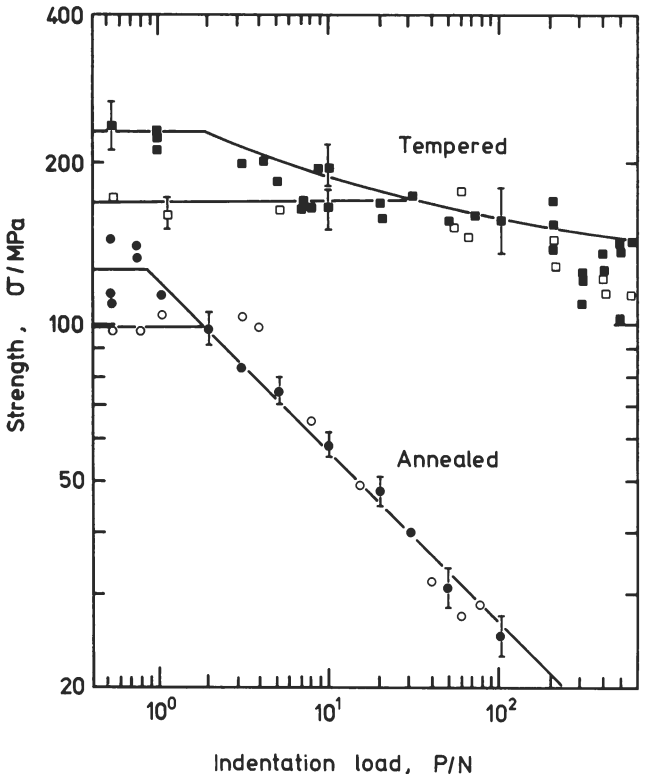

FIG. 2 Failure stress as a function of contact load for tempered and annealed soda-lime glass discs. Oil environment used to ensure equilibrium fracture conditions. Error bars represent standard deviation 8-10 tests. Closed symbols represent as-received surfaces, open symbols represent pre-abraded surfaces (320-mesh grit for tempered discs, 150-mesh for annealed discs). Cutoff strengths are zero-indentation values (mean).

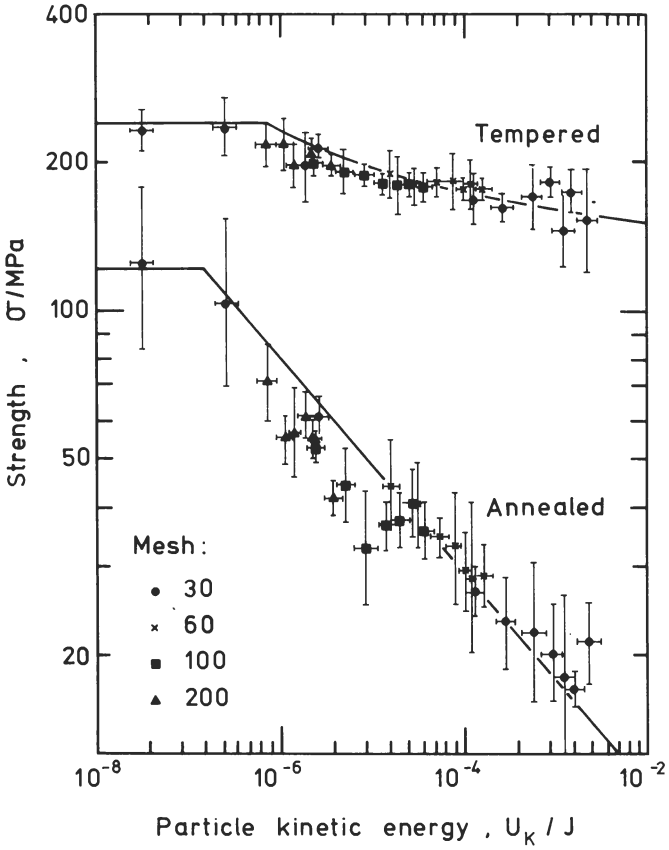

FIG. 3 Failure stress as function of particle kinetic energy for tempered and annealed soda-lime glass discs. Oil environment imposed immediately after impact stage. Error bars are standard deviations 4 discs. All discs tested with surfaces in as-received state.

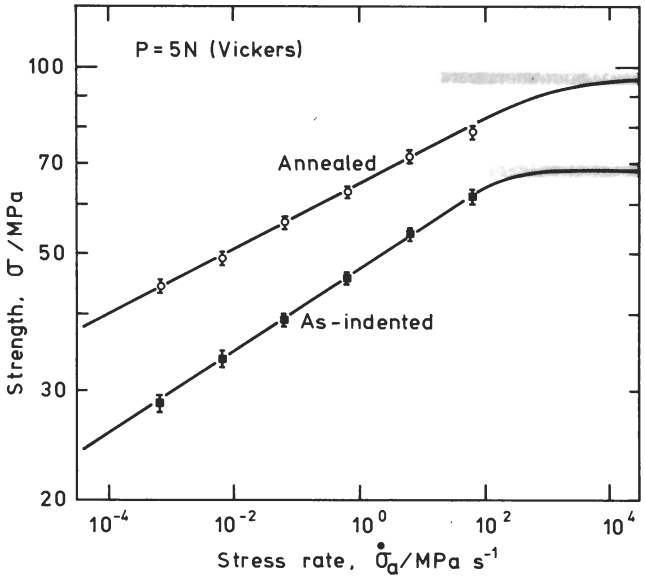

FIG. 4 Dynamic fatigue response for indented soda-lime glass discs broken in water environment. Error bars are standard deviations 10-30 specimens. Shaded regions indicate inert-strength levels.

in the two-stage test procedure[12]. Consequently, particle kinetic energy U_K replaces indentation load P as the abscissa in the figure. In this case, sieved SiC grit was accelerated onto a small, central target area of the disc test-pieces via a gas stream; estimates of particle mass from the grid mesh size ("equivalent spherical particle") and impact velocity from the gas stream monitoring system were used to determine a representative impact energy for each run.* The curves in Fig. 3 obtain directly from those fitted in Fig. 2, using an evaluation of Eq. (5) appropriate to Vickers geometry as the basis of conversion.

Next, Fig. 4 shows results for strength under conditions of dynamic fatigue[13]. The data are for tests in a water environment, to which all silicate glasses are highly susceptible in their fracture response. Two sets of data are plotted, for a single prescribed indentation load. "As-indented" specimens correspond to discs tested according to the normal indentation/strength procedure, in which case the residual contact stresses remain unaffected by the interval between the two stages ($\chi_r > 0$). "Annealed" specimens correspond to discs given an anneal treatment *between* the two stages, thereby removing the residual stresses ($\chi_r = 0$). In this figure, the curve through the data for annealed specimens is a fit in accordance with Eq. (11), obtained by matching to equilibrium strength values at high stress rate and adjusting the parameters to the power-law crack-velocity function. The curve through the data for as-indented specimens is then a prediction of Eq. (11) using the same adjusted parameters, but with the residual-stress term now included. These results serve to illustrate the magnitude of the residual-stress effect in the strength characteristics.

3.2 Other Ceramics

Equilibrium strength data were obtained as a function of static indentation load for a number of practically useful ceramics. The results are shown in Figs. 5 and 6. All materials except one were fine-grained relative to the scale of the radial crack pattern ($c \gtrsim 20$ μm typically); the exception was zirconia, with a grain size ~ 50 μm. The test pieces for flexural testing were all received with machined surfaces.

Fig. 5 shows results for several grades of alumina. Linear fits to Eq. (10) are again made in the high-load region for those materials free of pre-existing surface stresses. The curve for oil-quenched AℓSiMag corresponds to a temper stress σ_R = 106 MPa in the speci-

*Note, multiple impact is not cumulative in the strength degradation, contrary to the surface erosion and wear properties.

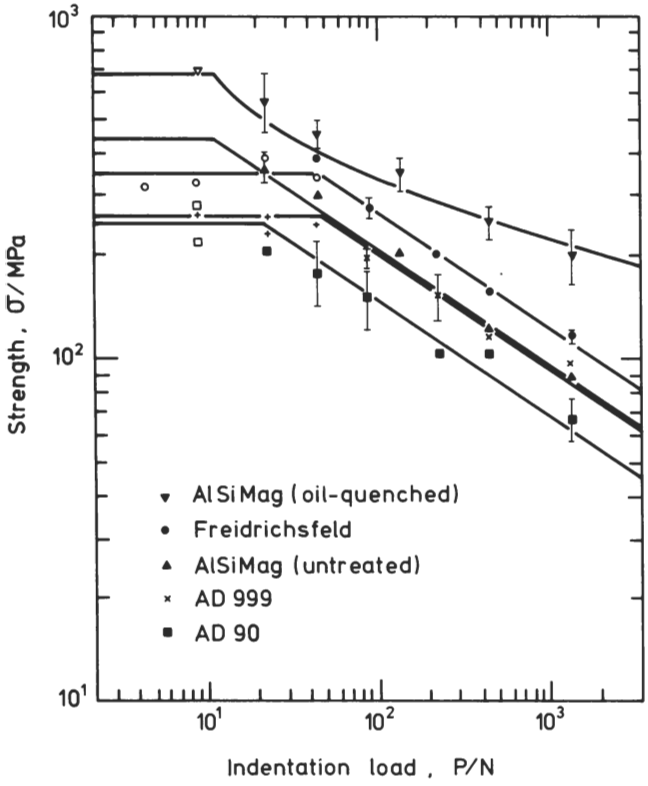

FIG. 5 Equilibrium failure stress as function of contact load for fine-grained aluminas. Cutoff strengths are zero-indentation values (mean) for machined surfaces. In this plot the open symbols indicate failures that did not *occur at indentation sites. Error bars are standard deviations 4-10 tests.*

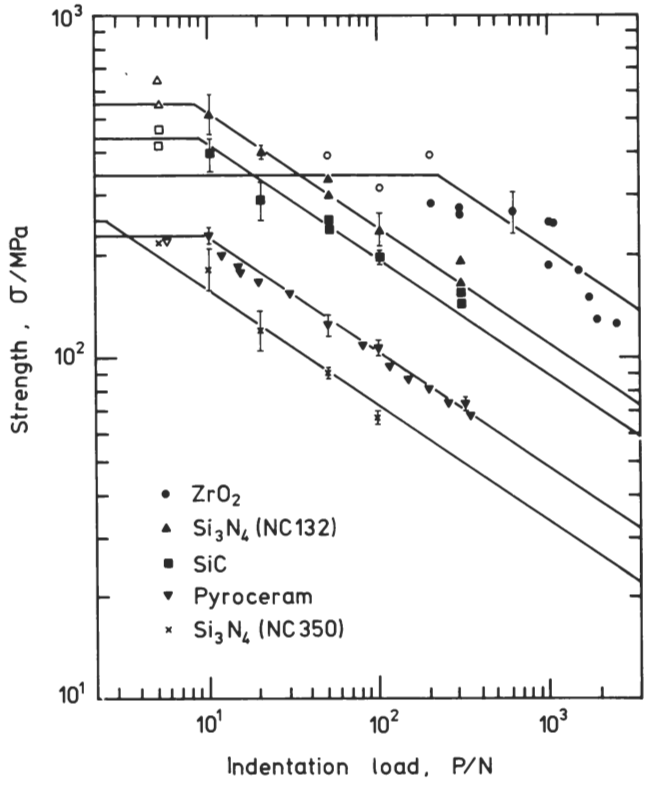

FIG. 6 Equilibrium failure stress as function of contact load for various ceramics (machined surface finish). Error bars are standard deviations 5 tests.

men surface[16]. It is interesting to note that the strengths of the materials "off the shelf" do not provide a reliable guide to relative performances under severe contact conditions. It appears that strength gains of about a factor of two are attainable in aluminas by proper optimisation of microstructural and compositional variables.

Finally, Fig. 6 compares the indentation/strength characteristics for two types of silicon nitride, silicon carbide, zirconia and a glass-ceramic (pyroceram). The relative merits of each material are again apparent in the high- and low-load regions. Zirconia is worthy of special mention in this regard. At low loads this material does not rate highly, due to its large grain size (which controls the pre-existent flaw population)[17]; however, at high loads its superior intrinsic toughness elevates it to the highest rank of all the ceramics tested.

4 Discussion

The theory and results presented above show the method of controlled indentation flaws to have certain virtues in the strength evaluation of brittle ceramics: (i) the procedure is simple, requiring only the availability of standard hardness- and strength-testing facilities; (ii) there is no need for microscopic measurement of the flaw ultimately responsible for failure, whether indentation-induced or pre-existent; (iii) resort to a statistical description of strength is avoided; (iv) the advantages of special material treatments, e.g. tempering, are readily evaluated. There would appear to be special relevance of the method to applications in which components are likely to encounter strength-degrading contact events during service. As we have seen, an "off-the-shelf" strength may not be a good indicator of ultimate performance. In this context it is worth emphasising that there is little point in taking excessive care to produce components with surfaces relatively free of flaws (unless attendant protective measures are taken, as in the production of optical fibres) — a subsequent errant sharp-particle contact event has the potential of initiating and propagating its own flaw, regardless of the initial state of surface perfection. Perhaps the most important practical manifestation of this type of behaviour is in high-velocity impact with atmospheric dust particles (radomes, turbine blades, I.R. windows, etc)[12]; a static-indentation investigation, in conjunction with Eq. (5), then allows for straightforward prediction of the impact response without ever having to gain access to complex impact apparatus.

Thus far we have not given explicit attention to the role of material parameters in strength characterisation. To examine this aspect, a plot of $\sigma P^{1/3}$ (best-fit values to equilibrium indentation/strength data, Figs. 2, 5, 6) vs $K_C^{4/3}(H/E)^{1/6}$ (Table 1) is given in Fig. 7. As predicted by Eq. (10), the plot is linear, notwithstanding the data uncertainties. The prime requirement for high strength under any contact conditions is a large toughness K_C. This type of diagram is useful for evaluating materials on a relative basis — clearly, the better-performance ceramics tend to the upper right of the plot. Again, one may invert the analysis, and use Fig. 7 as a calibration plot for estimating K_C from equilibrium strength data. From the error bars on the data points, an accuracy of ~ 20-30% could be expected in any such determination (note that uncertainties in the elastic/plastic parameter E/H will not contribute significantly to the error); this compares favourably with more conventional fracture mechanics procedures, which pay for higher accuracy with complexity in test-piece geometry. A similar approach may be applied to the dynamic fatigue results in Fig. 4; in particular, the data-fit analysis used to generate the curves in this figure provides an extremely accurate estimate of the crack-velocity exponent for the soda-lime-glass/water system, viz. $n = 17.9 \pm 0.5$. A critical evaluation of the indentation technique as a means of determining fundamental fracture parameters of brittle materials is currently under way in these laboratories.

Apart from their quantitative applications, indentation fracture systems offer valuable physical insight into the nature of microscopic flaws. In some respects the radial crack system may actually represent a close facsimile of the spurious handling-damage flaws which are known to exist in profusion on the typical brittle surface[1]. The major advantage here is the controlled manner in which the radial-crack evolution may be followed in terms of a well-defined driving force[7-9]. Of particular importance in this context is the significant role of irreversible-deformation processes in the fracture response, as manifested in the residual-stress contribution; the difference between the two sets of data in Fig. 4 is a clear illustration of this point. Failure to allow for the existence of residual contact stresses can accordingly lead to substantial systematic errors in strength analysis, especially in those situations where short-term data from macroscopic crack systems are used to

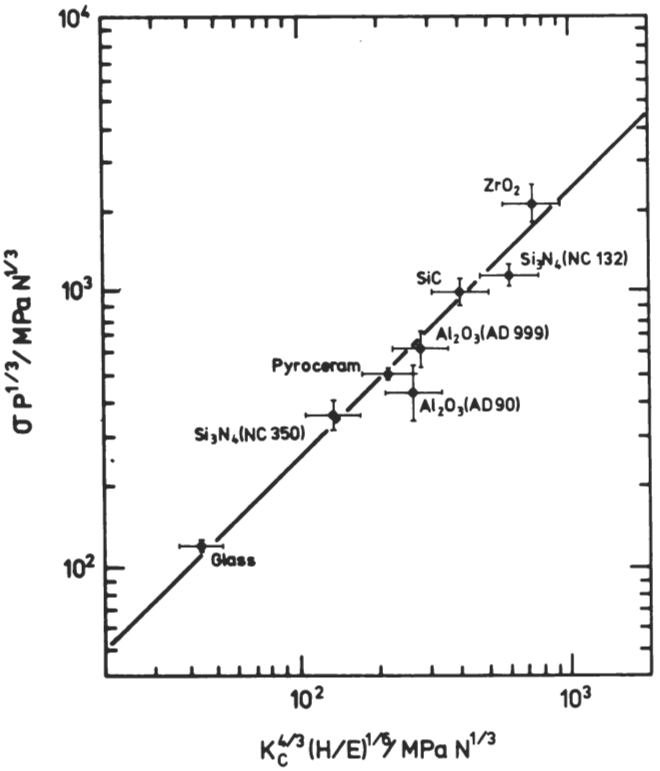

FIG. 7 Plot of indentation/strength data as function of material parameters. Straight line is curve fit to Eq. (10). Vertical error bars are standard deviations from curve fits, horizontal error bars are "typical" uncertainty levels in published material data.

predict long-term survival rates at high stress levels[3]. The apparent discrepancy between predicted and observed static fatigue characteristics of optical fibres[18] (where the flaw sizes approach the nm-scale) is just one important case where indentation testing can throw some light on flaw micromechanisms[19].

Acknowledgements

Parts of this work were carried out in collaboration with the Fracture and Deformation Division at the National Bureau of Standards, Washington D.C., U.S.A., under the direction of S.M. Wiederhorn. Funding for the program at U.N.S.W. was provided by the Australian Research Grants Committee and the Australian Department of Defence.

References

1. B.R. Lawn and T.R. Wilshaw, "Fracture of Brittle Solids" (Cambridge University Press, London, 1975).
2. "Fracture Mechanics Applied to Brittle Materials" (A.S.T.M. Special Technical Publication 678, Philadelphia, Pa, 1979).
3. S.M. Wiederhorn, pp. 635-665 in "Ceramics for High Performance Applications" (Brook Hill Publishing Co., Chestnut Hill, Mass., 1974).
4. B.R. Lawn and T.R. Wilshaw, J. Mater. Sci. **10** (1975) 1049.
5. B.R. Lawn and D.B. Marshall, pp. 205-229 in "Fracture Mechanics of Ceramics" (Plenum, New York, 1978).
6. B.R. Lawn and D.B. Marshall, J. Amer. Ceram. Soc. **62** (1979) 347.
7. D.B. Marshall and B.R. Lawn, J. Mater. Sci. **14** (1979) 2001.
8. D.B. Marshall, B.R. Lawn and P. Chantikul, J. Mater. Sci. **14** (1979) 2225.
9. B.R. Lawn, A.G. Evans and D.B. Marshall, J. Amer. Ceram. Soc., in press.
10. B.R. Lawn and M.V. Swain, J. Mater. Sci. **10** (1975) 113.
11. J.T. Hagan and M.V. Swain, J. Phys. D.: Appl. Phys. **11** (1978) 2091.
12. S.M. Wiederhorn and B.R. Lawn, J. Amer. Ceram. Soc. **62** (1979) 66; B.R. Lawn, D.B. Marshall and S.M. Wiederhorn, ibid, p. 71.
13. D.B. Marshall and B.R. Lawn, J. Amer. Ceram. Soc., in press.
14. J.R. Roark, "Formulas for Stress and Strain" (McGraw-Hill, New York, 1965).
15. D.B. Marshall and B.R. Lawn, J. Amer. Ceram. Soc. **61** (1978) 21.
16. D.B. Marshall, B.R. Lawn, H.P. Kirchner and R.M. Gruver, J. Amer. Ceram. Soc. **61** (1978) 271.
17. R.C. Garvie, R.H.J. Hannink, R.R. Hughan, N.A. McKinnon, R.T. Pascoe and R.K. Stringer, J. Aust. Ceram. Soc. **13** (1977) 8.
18. J.E. Ritter and K. Jakus, J. Amer. Ceram. Soc. **60** (1977) 171.
19. T.P. Dabbs, D.B. Marshall and B.R. Lawn, J. Amer. Ceram. Soc., in press.

Appendix

Key to Symbols

a	Half-diagonal of hardness impression.
c	Radial crack dimension
c_0	Post-indentation radial crack dimension (equilibrium conditions)
c_0'	Post-indentation radial crack dimension (kinetic conditions)
c_f	Radial crack dimension at failure (kinetic conditions)
c_m	Radial crack dimension associated with maximum in applied-stress/crack-size function.
E	Young's modulus
H	Mean indentation pressure – "hardness"
K	Stress intensity factor
K_C	Critical stress intensity factor – "toughness"
K_a	Stress intensity factor associated with applied tensile field
K_r	Stress intensity factor associated with residual contact field
n	Exponent in power-law crack-velocity function
P	Peak indention Load
t	Time
t_f	Time to failure (kinetic fracture conditions)
U_K	Kinetic energy of indenting particle
v	Crack velocity
v_0	Crack-velocity constant
α_0	Indentation constant associated with hardness impression
β_0	Indentation constant associated with radial crack system
$\S R$	Indentation constant associated with radial crack system
σ	Critical value of applied stress at failure – "strength"
σ_a	Applied tensile stress on radial crack
σ_m	Maximum in applied-stress/crack-size function
σ_R	Residual temper stress
χ_r	Indentation constant associated with radial crack system
ψ	Characteristic indenter angle
Ω	Crack-geometry constant